Pharm Res (2014) 31:2952–2962
DOI 10.1007/s11095-014-1390-7

RESEARCH PAPER

Cerium Oxide Nanoparticles Inhibit Adipogenesis in Rat Mesenchymal Stem Cells: Potential Therapeutic Implications

Antonella Rocca • Virgilio Mattoli • Barbara Mazzolai • Gianni Ciofani

Received: 17 December 2013 / Accepted: 15 April 2014 / Published online: 8 May 2014

ABSTRACT

Purpose Cerium oxide nanoparticles (nanoceria, NC) have extraordinary antioxidant activity that made them suitable as a therapeutic agent for several diseases where reactive oxygen species (ROS) act by impairing the normal redox balance. Among different functions, it has been proven that ROS are cellular messengers involved in the adipogenesis: we thus investigated the implication of NC administration in the potential inhibition of adipogenic differentiation of mesenchymal stem cells (MSCs) used as a model of adipogenesis.

Methods We evaluated cytotoxic effects and adipogenic maturation of mesenchymal stem cells following *in vitro* NC administration, both at gene and at phenotype level.

Results Overall, our results demonstrated that NC efficiently inhibit the maturation of MSCs toward adipocytes owing to their ability to reduce the production of the ROS necessary during adipogenesis.

Conclusions These findings, even if preliminary, represent an important step toward the potential pharmaceutical application of NC in the treatment of obesity.

KEY WORDS Adipogenesis · Cerium oxide nanoparticles · Mesenchymal stem cells · Reactive oxygen species

Electronic supplementary material The online version of this article (doi:10.1007/s11095-014-1390-7) contains supplementary material, which is available to authorized users.

A. Rocca • V. Mattoli • B. Mazzolai • G. Ciofani (✉)
Istituto Italiano di Tecnologia, Center for Micro-BioRobotics @SSSA Viale Rinaldo Piaggio 34, 56025 Pontedera, Pisa, Italy
e-mail: gianni.ciofani@iit.it

A. Rocca (✉)
Scuola Superiore Sant'Anna, The BioRobotics Institute, Viale Rinaldo Piaggio 34, 56025 Pontedera, Pisa, Italy
e-mail: antonella.rocca@iit.it

ABBREVIATIONS

MSC	Mesenchymal stem cell
NC	Nanoceria
qRT-PCR	Quantitative real time reverse transcriptase-polymerase chain reaction
ROS	Reactive oxygen species

INTRODUCTION

Cerium oxide nanoparticles (nanoceria, NC) are considered an ideal inorganic antioxidant, owing to their self–regenerative capability of free radical scavengers (1). These nanoparticles in fact show interesting redox activity because of the presence of crystalline defects on their surface, that allow for the presence of both Ce^{4+} and Ce^{3+} species (2).

Many studies confirmed that, in biological contexts, nanoceria exhibit antioxidant effects, owing both superoxide dismutase (3–5) and catalase (6) mimetic activities. Recently, our group showed that the reactive oxygen species (ROS) scavenging property of nanoceria positively affects neuronal differentiation and dopamine production in PC12 cells (7, 8). Moreover, nanoceria have been widely investigated for the treatment of several disorders, including cardiomyopathy (9), cancer (10), and in the treatment of injuries of the spinal cord (11). To date, several antioxidant therapies were developed to reduce the ROS production involved in the pathogenesis of various diseases; however, traditional antioxidant agents like vitamins (12), nitrones (13) and exogenous superoxide dismutases (SODs) (14) suffer of some limitations ranging from enzymatic degradation, to the difficulty to reach the target, and to their short half-life. It is therefore clear that the growing interest on nanoceria is due to their antioxidant auto-regenerative ability (15).

One of the proposed models that explain this activity suggests that Ce^{3+} reduce superoxide forming H_2O_2 and

Ce^{4+}, while H_2O_2 and Ce^{4+} restore Ce^{3+} and develop O_2 (16). The NC auto-regenerating antioxidant activity made them thus suitable to finely control ROS levels in cells, tissues, and, ultimately, organisms (17). ROS are in fact generally associated with negative effects, because oxidative damages to proteins and nucleic acids are often at the base of important pathologies like cancer and neurodegenerative diseases (18). However, in some cases, ROS may have many physiological roles, including signaling and control of inflammatory response and cell proliferation (19), thus their tuning through NC administration has to be carefully evaluated.

Among different pathological conditions, several studies have pointed out a correlation between oxidative stress and adiposity (20–22). The mechanisms through which ROS promote adipocyte maturation are still not completely clear, but it has been demonstrated that mitotic clonal expansion during adipocyte differentiation is accelerated by oxidant treatment (23). A study reported that the link between fat accumulation and ROS is the protein PKCβ, which, once activated by oxidative species, induces the adipogenic process (24).

Excessive fat accumulation (25), better known as obesity, affects 11% of the world population (data from World Health Organization statistics, 2008). Obesity is often associated with several metabolic disorders (diabetes, hypertension, *etc.*), commonly defined together as "metabolic syndrome", that increase the risk of mortality (26). In the recent years, many methods have been approached to reduce fat accumulation in obese patients, such as physical activity, diet, surgery, and pharmacotherapies (27). However, sometimes lifestyle modification and pharmacologic treatment are not enough to achieve a significant weight loss (28).

In this study, we investigated the effects of the antioxidant activity of nanoceria in reducing the capability to differentiate into adipocytes of mesenchymal stem cells, used as model of adypogenesis (29): our purpose is to demonstrate the inhibition of adipogenesis induced by nanoceria in order to exploit these nanoparticles in potential therapeutic treatments of obesity.

MATERIALS AND METHODS

Cerium Oxide Nanoparticles

Cerium oxide nanoparticles were purchased from Sigma (544841), and extensively characterized in previous works (7, 8). They appear as a powder of quite dispersed size distribution (5–80 nm), with a cubic crystalline structure, high purity, and a Ce^{3+} content of ~23%, suitable for an optimal NC redox activity. Nanoparticles were dispersed through a mild sonication in ultrapure MilliQ water (Millipore) at a concentration of 10 mg/ml, and then diluted in the cell culture medium at the desired concentrations just before the experiments. Particle size distribution and Z-potential of NC in cell culture medium were analyzed with a Nano $\mathcal{Z}$-Sizer 90 (Malvern Instrument).

Cell Culture

Rat mesenchymal stem cells (MSCs), isolated from bone marrow, were purchased from Lonza (PT2505) and grown in expansion medium, constituted by high glucose Dulbecco's Modified Eagle's Medium (DMEM) supplemented with 10% fetal bovine serum (FBS), 100 U/ml penicillin, 100 mg/ml streptomycin, and 200 mM glutamine. Cells were splitted with trypsin treatment at 80% of confluence, and used for all experiments within the fifth passage.

Table I Primer sequences of target and housekeeping genes.

Gene	Symbol gene	Sequence (5′–3′)
Peroxisome proliferator-activated receptor gamma	*Pparg*	F – GACCCAATGGTTGCTGATTAC
		R – GGACGCAGGCTCTACTTT
Glycerol-3-phosphate dehydrogenase 1	*Gpd1*	F – AGTTCTGTGAGACGACCATT
		R – CACTGTGTCCACCTCTTGTA
CCAAT/enhancer binding protein (C/EBP), alpha	*Cebpa*	F – GATAAGAACAGCAACGAGTACC
		R – GTCAACTCCAACACCTTCTG
Lipoprotein lipase	*Lpl*	F – GCCCAGCAACATTATCCAG
		R – GGGGTAGTTAAATTCTTCCTCCA
cAMP response element-binding protein 1	*Creb1*	F – ATTCTACAATATGCACAGACCACT
		R – CCAGAGGCAGCTTGAACA
Glyceraldehyde-3-phosphate dehydrogenase	*Gapdh*	F – AACCTGCCAAGTATGATGAC
		R – GGAGTTGCTGTTGAAGTCA-3′
Ribosomal protein, large, P0	*Rplp0*	F – TACCATTGAAATCCTGAGCGA
		R – ATCAGCCCGAAGGAGAAG

Cytocompatibility Investigation

Cell proliferation was evaluated with the WST-1 assay ((2-(4-iodophenyl)-3-(4-nitophenyl)-5-(2,4-disulfophenyl)-2H-tetrazoilium monosodium salt, provided in a pre-mix electro-coupling solution, BioVision). Cells were seeded in 96-wells plate at a density of 6,000/cm^2 (n=6) and, after 24 h, they underwent a treatment with 0, 10, 20, 50 and 100 µg/ml of NC, for 3, 6 and 10 days in expansion medium. At each time point, medium was replaced with 100 µl of the fresh medium supplemented by 10 µl of the WST-1 solution, and absorbance at 450 nm was read after 90 min of incubation with a microplate reader (Victor3, Perkin Elmer).

Live/Dead® Viability/Cytotoxicity Assay Kit (Molecular Probes) was used to assess viability of the cell cultures after 10 days of NC treatment. This fluorescence assay is based on cellular staining by calcein AM and ethidium homodimer (EthD-1). The first probe labels in green live cells because of the enzymatic conversion of non-fluorescent calcein AM to the green-fluorescent calcein; the second probe labels dead cells in red, binding to nucleic acids of cells with compromised membranes. For this test MSCs were seeded in 24-wells plate at the density of 6,000/cm^2 and treated as previously described. After 10 days of proliferation, cell cultures were rinsed with PBS and then incubated with 2 µM calcein AM, 4 µM EthD-1 and 5 µg/ml Hoechst 33342 (for nucleus

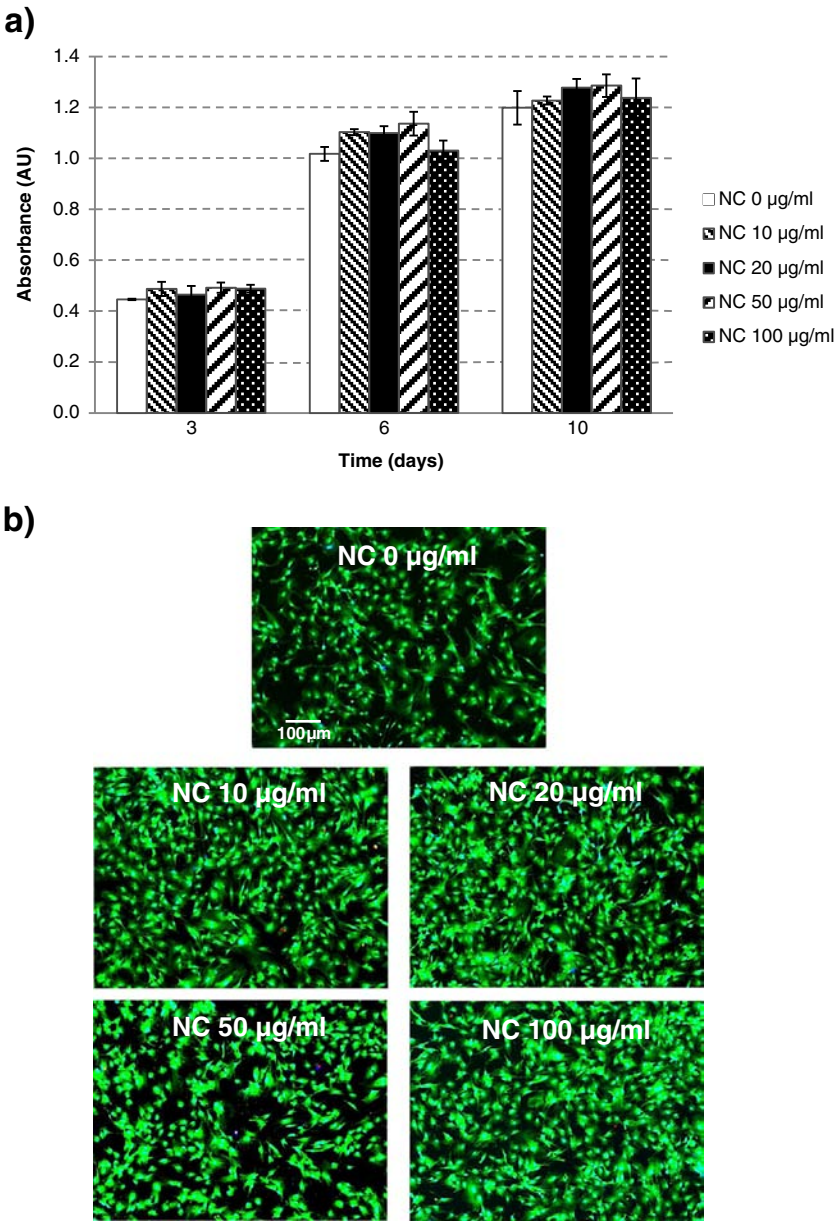

Fig. 1 Results of WST-1 assay performed after 3, 6 and 10 days in the presence of 0, 10, 20, 50 and 100 µg/ml of NC (n=3) (**a**); Live/Dead® assay on MSCs incubated with increasing concentrations of NC after 10 days (*red*: dead cells; *green*: live cells; *blue*: nuclei) (**b**).

counterstaining in blue) in 1 ml of expansion medium for 5 min at 37°C before observation under an inverted fluorescence microscope (Eclipse TI, Nikon) equipped with a cooled CCD camera (DS-5MC USB2, Nikon).

Evaluation of the Interaction Between Nanoceria and MSCs

Cytoskeleton/focal adhesion staining Kit (Millipore) was used for the evaluation of the distribution of actin filaments and the development of cell focal adhesions. The kit includes: TRITC-conjugated phalloidin, that stains in red cytoskeletal f-actin filaments; a mouse monoclonal antibody against vinculin, a cytoskeletal protein involved in the focal adhesion of cells to substrates; a DAPI solution for nucleus blue counterstaining. Cells (6,000/cm^2 in 24-wells plate, incubated for 10 days with 0–100 μg/ml of NC) were fixed with 4% paraformaldehyde in PBS for 20 min at 4°C, permeabilized with 0.1% Triton X-100 (Sigma) for 15 min, and treated with a blocking solution (10% goat serum in PBS) for 1 h before incubation with the vinculin primary monoclonal antibody (diluted 1:100 in 10% goat serum) for 45 min. Thereafter, cells were incubated with the staining solution constituted by a green fluorescent labeled secondary antibody (AP124F from Millipore, diluted 1:50 in 10% goat serum), 100 μM FITC-phalloidin, and 1 μM DAPI. After extensive washing steps, samples were observed with the fluorescence microscope and acquired images elaborated with the ImageJ software (http://rsb.info.nih.gov/ij/).

Scanning electron microscopy (SEM) was performed on MSCs incubated with NC 20 μg/ml for 10 days. Cells were fixed with 4% paraformaldehyde in PBS for 30 min at 4°C, followed by a further incubation with a 2.5% glutaraldehyde in de-ionized water for 2 h at 4°C. Thereafter, samples were dehydrated with a series of steps in ethanol at increasing concentrations (0, 25, 50, 75 and 100%) and air-dried for 24 h. Finally, before observation at the SEM (Helios NanoLab 600i, FEI) samples were sputter-coated with a thin gold layer. Elemental microanalysis was also carried out through Energy Dispersive X-ray spectroscopy (EDX, Bruker), in order to assess presence of cerium (*i.e.*, nanoparticles) accumulation in association to the cells.

Cerium oxide nanoparticle internalization was assessed through laser scanning confocal microscopy. Cells (seeded at a density of 6,000/cm^2 on Ibidi 60 μ-Dish 35 mm), were treated for 12 h with 20 μg/ml of Oregon green-labeled NC (obtained as reported in a previous work (8)), and thereafter incubated with a medium supplemented with Vibrant® DiO (a membrane red marker, V-22886 from Molecular Probes, 5 μl each 1 ml of medium) and Hoechst 33342 (1 μl each 1 ml of medium). The cells were finally observed under a confocal laser scanning microscope (C2s, Nikon).

MitoTracker® (M22425 form Molecular Probes) and LysoTracker® (L7528 from Molecular Probes) staining were performed to assess possible NC co-localization in cellular compartments, in samples treated for 3 days with 20 μg/ml of Oregon green-labeled NC. For mitochondria staining, samples were incubated with 500 nM of probe and Hoechst 3342, while for lysosome detection, LysoTracker® was used on the samples at a concentration of 100 nM jointly to Hoechst 33342. Finally, samples were observed under confocal microscope.

Adipogenic Differentiation

In order to induce adipogenic differentiation, cells were seeded at a density of 6,000/cm^2 in 24-wells plate, and incubated with 0, 20, and 50 μg/ml of NC for 14 days with high glucose DMEM supplemented with 10% FBS, 100 U/ml penicillin, 100 mg/ml streptomycin, 200 mM L -glutamine, 5 μg/ml insulin, 1 μM dexamethasone, 20 μM indomethacin, and 500 μM 3-isobuty-l-methyl-xanthine.

The gene transcription of specific adipogenesis markers (peroxisome proliferator-activated receptor gamma, *Pparg*, glycerol-3-phosphate dehydrogenase 1, *Gpd1*, CCAAT/enhancer binding protein alpha, *Cebpa*, lipoprotein lipase, *Lpl*, and cAMP response element-binding protein 1, *Creb1*), was evaluated through quantitative real time RT-PCR (qRT-PCR). At this aim, RNA was extracted with the High Pure RNA Isolation Kit (Roche) following the manufacturer's protocol, and quantified at 260 nm with a spectrophotometer

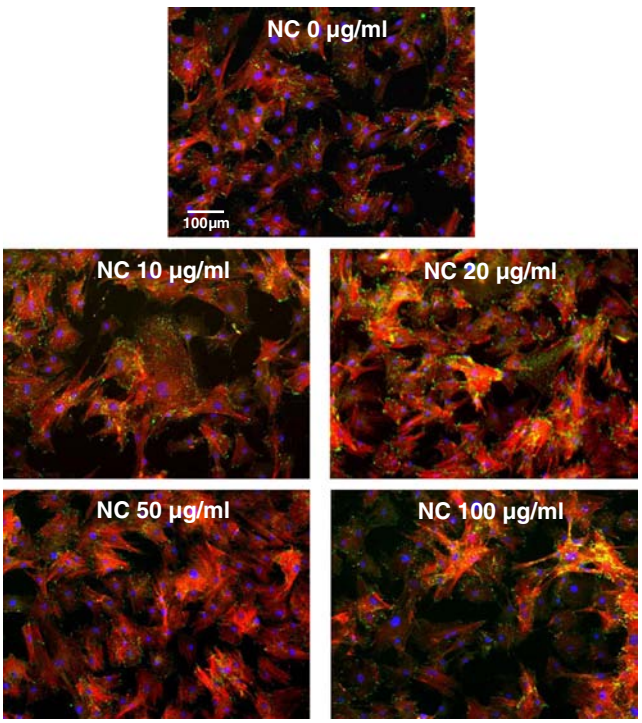

Fig. 2 Immunofluorescence staining of vinculin (*green*) and f-actin (*red*) in proliferating mesenchymal stem cells after 10 days of incubation witch increasing NC concentrations. Nuclei counterstained in blue.

(Lambda 45, Perkin Elmer). For each sample, 100 ng of extracted RNA were reverse-transcribed into cDNA through iScriptTM Reverse Transcription Supermix (Bio-Rad). The RNA was divided into two aliquots: one part of the sample was used for the reverse transcription, while the other part was used as an elimination control of any contaminating genomic DNA (negative control without reverse transcriptase). The reverse transcription reaction was performed by adding 4 µl of 5x iScript reaction mix (Bio-Rad) to the appropriate amount of RNA solution and nuclease-free water for a final volume of 20 µl. The reaction protocol included an initial incubation at 25°C for 5 min, followed by consecutive incubations at 42°C for 45 min, at 48°C for 15 min, and finally at 85°C for 5 min to inactivate the reaction. The volume was finally increased up to 200 µl with MilliQ water.

The amplification reactions were performed on a thermocycler CFX Connect™ Real-Time PCR Detection System (Bio-Rad), with verification of the specificity of products amplified by melting curve analysis. Each amplification reaction was set up in 20 µl, that comprise 10 µl of SsoAdvancedTM SYBRGreen® Supermix (Bio-Rad), 1 µl of primer solution (forward and reverse primers 8 µM), 4 µl of MilliQ water, and 5 µl of diluted cDNA. In each experiment the possible DNA contamination was determined by introducing an internal control where cDNA was omitted from the reaction mixture and replaced by MilliQ. The temperature protocol used was the following: one cycle at 98°C for 30 s, 40 cycles at 98°C for 3 s and 60°C for 7 s, a temperature ramp from 65 to 95°C, with 0.5°C/s increments. The samples were analyzed in triplicate and the cycle threshold (C_t) value relative of control samples was adopted as reference for the calculation of $\Delta\Delta C_t$, *i.e.*, the difference between ΔC_t values deriving from difference between C_t of the target and of the housekeeping genes (*Gapdh* and *Rplp0*) for the subsequent samples. Primers sequences (forward and reverse) of the investigated genes are reported in Table I.

At the end of differentiation, AdipoRed™ Reagent (Lonza) was used to quantify intracellular lipid droplets accumulation thanks to its ability to become fluorescent in hydrophobic

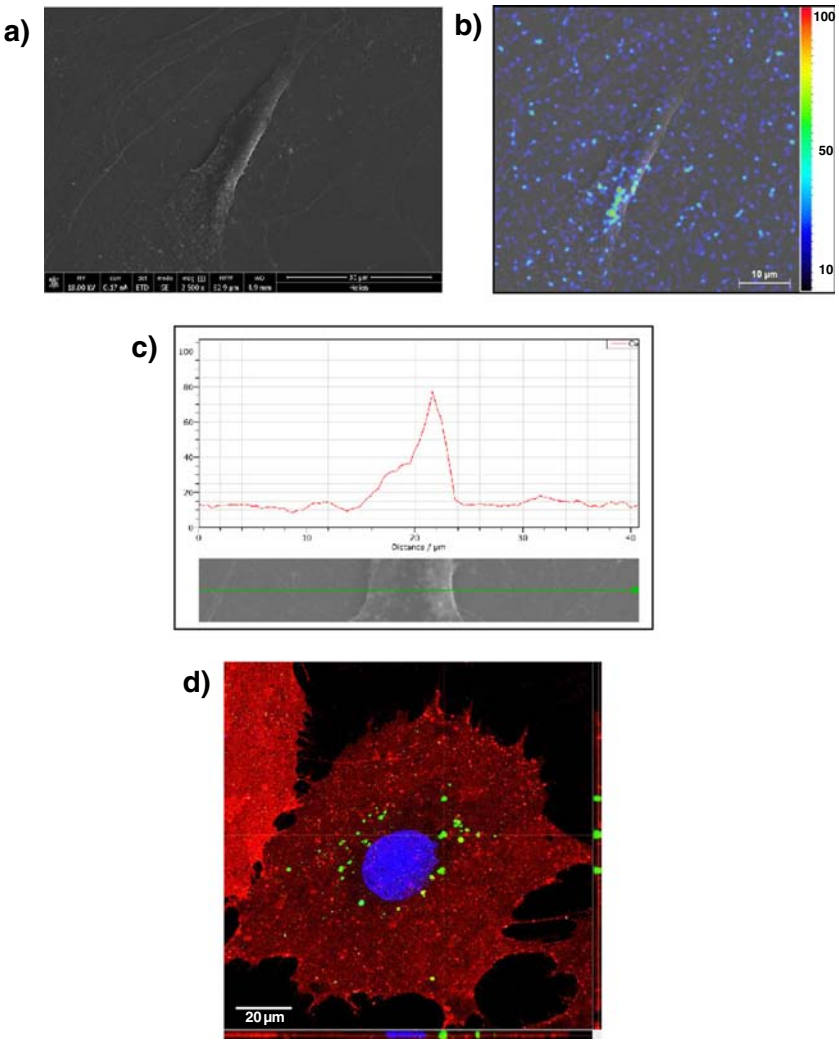

Fig. 3 Analysis of the interactions between MSCs and NC (20 µg/ml) after 10 days of proliferation: scanning electron microscopy (**a**); scanning electron microscopy overlapped to elemental map (**b**); elemental microanalysis (**c**). Laser confocal microscopy of cell membrane (*red*) and nuclei (*blue*) after 12 h of incubation with Oregon green-labeled nanoparticles (*green*) (**d**).

compartments, in particular in triglycerides enriched environments. Samples were rinsed with PBS and incubated with 30 µl of the marker in 1 ml of PBS for 10 min at 37°C. Finally, cultures were observed under fluorescence microscope.

As a further assessment of adipocyte maturation, glycerol-3-phosphate dehydrogenase (G3PDH) activity was quantified though a specific assay kit (ab174095 from Abcam) that detects the activity of this enzyme, that is crucial for the lipid metabolism. The assay measures the absorbance at 450 nm of a colored probe produced by an intermediate formed by the reaction between G3PDH and the substrate. Cell pellets at 14 days of differentiation were lysed and centrifuged. Thereafter, the supernatants of each sample ($n=3$) were used to assess G3PDH activity following manufacturer's instruction. The plate was incubated for 30 min at 37°C and the absorbance was read at 450 nm with a microplate reader (Victor3, Perkin Elmer).

Statistical Analysis

Statistical analysis of the data was performed with KaleidaGraph (Sinergy Software), using one-way analysis of variance (ANOVA) followed by *post-hoc* Bonferroni's test; qRT-PCR data were analyzed with Bio-Rad CFX Manager software. Differences were considered significant when p-values <0.05.

RESULTS

MSC Viability

Cytocompatibility assays were performed to assess any possible toxic effect on MSCs treated with increasing NC concentrations (0, 10, 20, 50 and 100 µg/ml) under proliferative conditions for up to 10 days.

Tested nanoparticles presented a mono-disperse distribution in the cell culture medium (98.0% peak at a size of 260 nm) and a slightly negative ζ-potential (about -5 mV). Similar results were observed for the fluorescent labeled NC used for confocal analysis (95.0% peak at a size of 210 nm, ζ-potential ~–5 mV).

Cells incubated with NC were quantitatively analyzed through cellular viability assay WST-1, and qualitatively with the Live/Dead® assay. Results of WST-1 performed after 3, 6 and 10 days showed no statistically significant differences ($n=3$, $p>0.05$) with respect to the control, at each concentration and at each time-point (Fig. 1(a)). Live/Dead® assay confirmed absence of significant cytotoxic effects on MSCs incubated with different NC concentrations (Fig. 1(b)), in terms of membrane integrity and qualitative morphological aspect. Overall, these results indicate that NC are not harmful for MSC viability and proliferation, and a regular metabolic activity has been observed on cells loaded with different NC concentrations after 10 days, with no appreciable differences against controls.

MSCs/NC Interaction

Immunofluorescence staining of cytoskeleton of proliferating mesenchymal stem cells also supported the evidence that cells are viable and that cytoskeleton does not present any appreciable qualitative alteration of its conformation. In Fig. 2 we can see immunostaining of vinculin (green), f-actin (red), and nuclei (blue).

Scanning electron microscopy images of MSCs incubated for 10 days with 20 µg/ml of NC demonstrated the presence

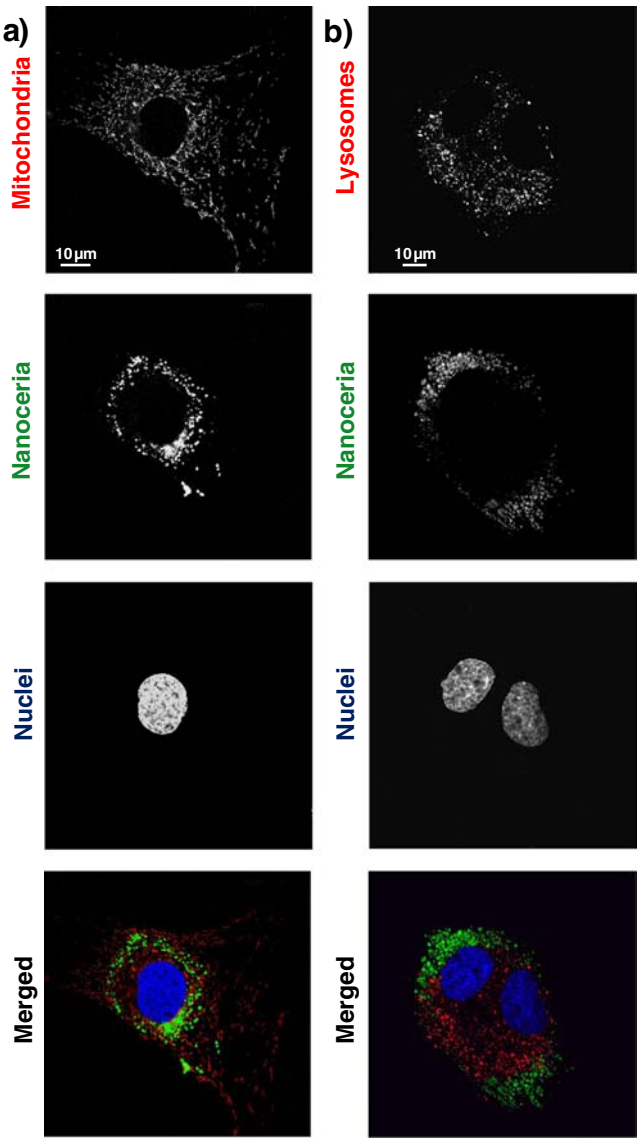

Fig. 4 MitoTracker® images of mitochondria (*red*), NC (*green*) and nuclei (*blue*) of MSCs after 3 days of proliferation in the presence of 20 µg/ml Oregon green-labeled NC (**a**); LysoTracker® images of lysosomes (*red*), nanoceria (*green*) and nuclei (*blue*) of MSCs after 3 days of proliferation in the presence of 20 µg/ml Oregon green-labeled NC (**b**).

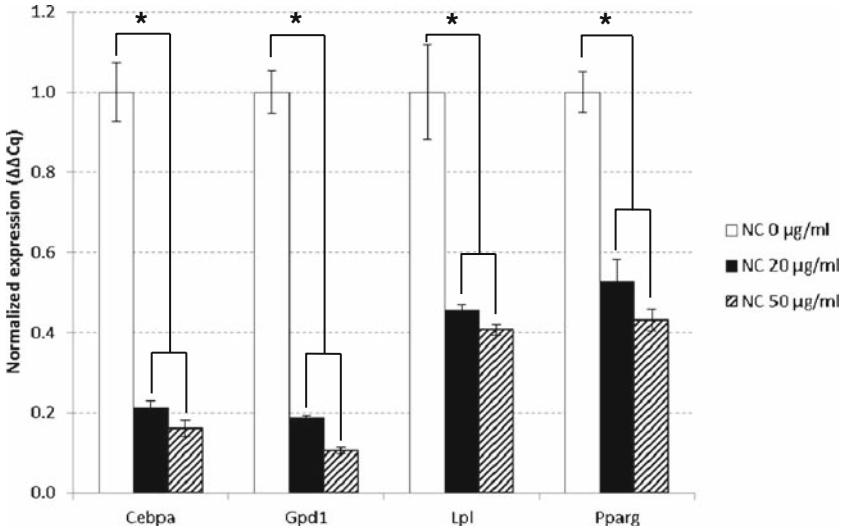

Fig. 5 Quantitative real time PCR of genes involved in the adipogenesis after a 14-day treatment with NC; *$p < 0.05$.

of nanoparticles associated to the cell membrane (Fig. 3(a)). The SEM image overlapped to the elemental map with pseudo–colors indicating the cerium concentration intensity suggests a strong interaction with the cells (Fig. 3 (b)). This is more clearly depicted in Fig. 3(c), where the profile of the cerium concentration provided by the elemental microanalysis is reported along a line virtually crossing the cell body (Fig. 3(c)).

Laser confocal microscopy eventually demonstrated as NC are indeed strongly internalized by the cells and, from Fig. 3 (d), we can appreciate green-labeled nanoparticles inside the cytoplasm (counterstained in red). This image is a slice from a *z*–stack, along with side projections showing as NC are actually in the inner of the cell. Furthermore, MitoTracker® and LysoTracker® staining images (Fig. 4(a) and (b), respectively) proved that NC do not co-localize with mitochondria or lysosomes, as demonstrated by the well separated color channels (NC in green, organelles in red). The absence of co–localization is definitely demonstrated by the estimation of the Pearson's coefficient ($R \sim 0$ for both mitochondria and lysosomes).

Taken together, all these results demonstrate a strong interaction between cells and NC, that are located both on the cell membrane and in the cytoplasm.

Adipogenic Differentiation

To assess the effects of NC in the regulation of the adipogenesis mechanism, we evaluated the adipocyte maturation first with quantification of transcribed genes, and then through the analysis of cell phenotype and functionality.

The results from qRT-PCR indicated a significant ($p < 0.05$) down-regulation of all the adipogenesis marker genes in cultures treated both with 20 µg/ml (*Pparg* 2-folds, *Gpd1* 5-folds, *Cebpa* 5-folds, *Lpl* 2-folds) and 50 µg/ml (*Pparg* 2-folds, *Gpd1* 9-folds, *Cebpa* 6-folds, *Lpl* 2.5-folds) of NC, when compared with control differentiated adipocytes (Fig. 5).

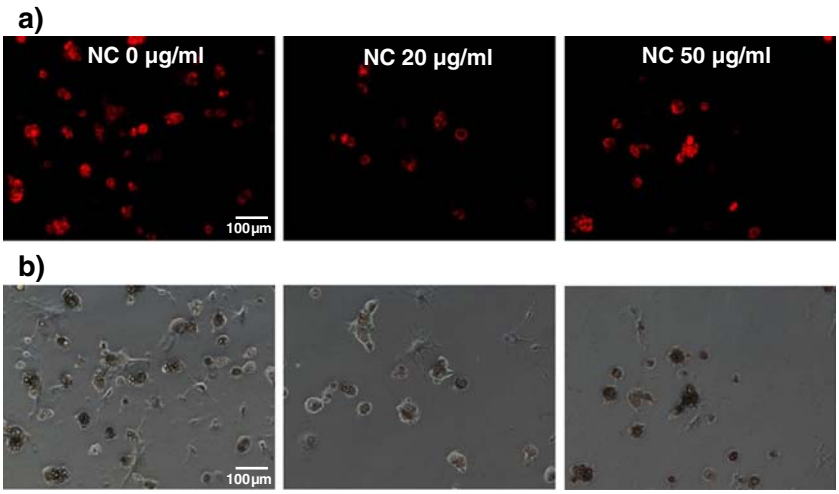

Fig. 6 Adipored™ assay after 14 days of differentiation of MSCs: lipid vesicles in red fluorescence (**a**); respective images in bright field (**b**).

Adipored™ assay demonstrated the presence of lipid vesicles (Fig. 6(a), in red) formed in the MSCs after a two-weeks treatment with the adipogenic medium. However, Fig. 6(a) shows a considerable decrement of fluorescent lipid droplets in the samples treated with NC, seeming the phenomenon to be, at least at a first qualitative evaluation, dose-dependent. To quantify the differentiation status, we evaluated the number of the cells presenting lipidic droplets over the total number of cells, confirming a significant reduction ($p<0.05$) of positive cells in samples treated with both 20 μg/ml of NC and 50 μg/ml (in both cases ~50%, Fig. 7(a)).

These results suggest that NC cause an inhibition of the accumulation of intracellular triglycerides, that is a hint of a significant reduced adipocyte differentiation. In order to withdraw functional quantitative data, activity of G3PDH was quantified, an enzyme typical of adipocyte late maturation. Interestingly, the assay proved that NC decreased the activity of this enzyme at both 20 and 50 μg/ml doses with respect to the control after 14 days of differentiation ($p<0.05$, Fig. 7(b)). The G3PDH activity was 0.218±0.076 mU/ml, 0.121±0.009 mU/ml and 0.051±0.014 mU/ml for control, NC 20 μg/ml and NC 50 μg/ml, respectively.

In order to gain an insight of the mechanisms at the base of our findings, we finally analyzed transcription of the gene encoding for Creb1, a transcription factor activated by ROS necessary to induce adipogenesis, that resulted significantly down-regulated (2-folds for the 20 μg/ml dose, 2.5-folds for the 50 μg/ml dose, in both cases $p<0.05$) following NC treatment (Fig. 8(a)). Taken together, these results definitely prove that NC are able to efficiently reduce the adipogenic differentiation of MSCs towards mature adipocytes, through a ROS scavenging action (further details about ROS inhibition are provided as Supplementary Material).

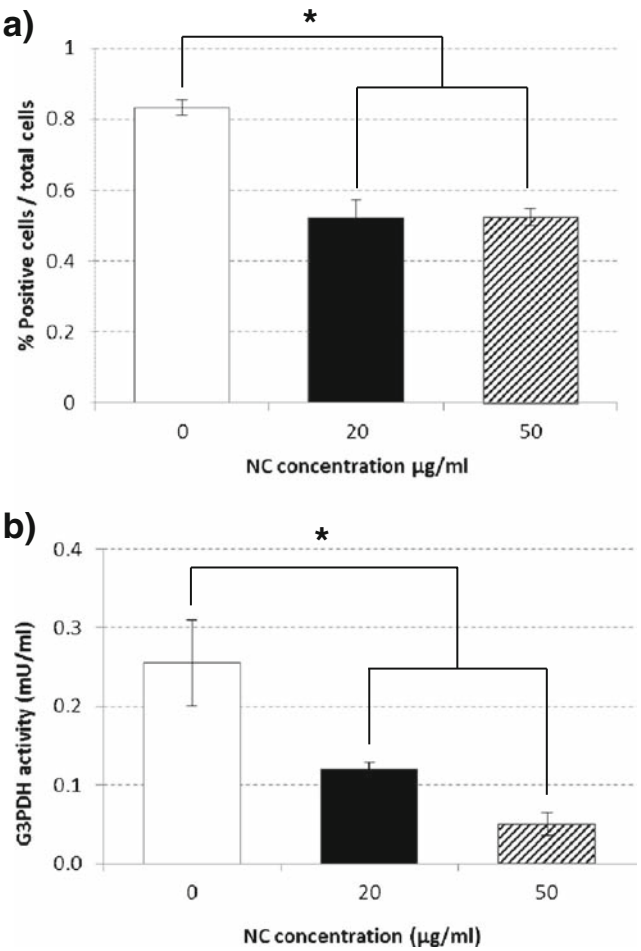

Fig. 7 Quantification of lipid droplet formation assessed after Adipored™ staining (**a**); quantitative evaluation of G3PDH activity in MSCs treated with increasing concentrations of NC after 14 days of differentiation (**b**); *$p<0.05$.

DISCUSSION

In vitro studies proved that nanoceria exhibit two complementary behaviors: while they generally have antioxidant effects prolonging the cell survival, on the other hand, at acidic pH values, they act as an oxidase, thus generating ROS (30). In this study, the antioxidant property of NC was examined as a potential agent of inhibition of adipogenesis in MSCs. It is in fact well established that MSCs are precursor of adipocytes, and they are an excellent model for the study of innovative therapies in the treatment of adiposity (31).

First of all, we confirmed the cytocompatibility of NC on MSCs. Other studies demonstrated that NC are not toxic for various cell lines (32–34), and even in the case of MSCs, NC up to 100 μg/ml do not present negative effects on the cells in terms of viability, proliferation, and cytoskeletal conformation. Thereafter, we assessed the interaction of NC with MSCs, revealing a strong membrane association (with SEM analysis) and internalization (with confocal microscopy) with a preferential distribution at the cytoplasm level, without co-localization in acidic compartments of the cells. NC are not distributed in mitochondria as instead reported by Singh *et al.* for keratinocytes (35); moreover, the absence of NC in the lysosomes avoids its pro-oxidant effects at acidic pH (36).

The evaluation of the gene expression of the differentiating samples treated with NC for 14 days demonstrated a significant decrement of the main adipogenesis marker genes with respect to the control. The examined genes for the induction of the adipogenic differentiation were *Pparg*, *Cebpa*, *Lpl* and *Gpd1*. Peroxisome proliferator-activated receptor gamma (coded by *Pparg*) is the key transcription factor that induces adipocyte differentiation (37), and its product induces the expression of the gene CAAT/enhancer-binding protein alpha (*Cebpa*), by binding its promoter. Together, *Pparg* and

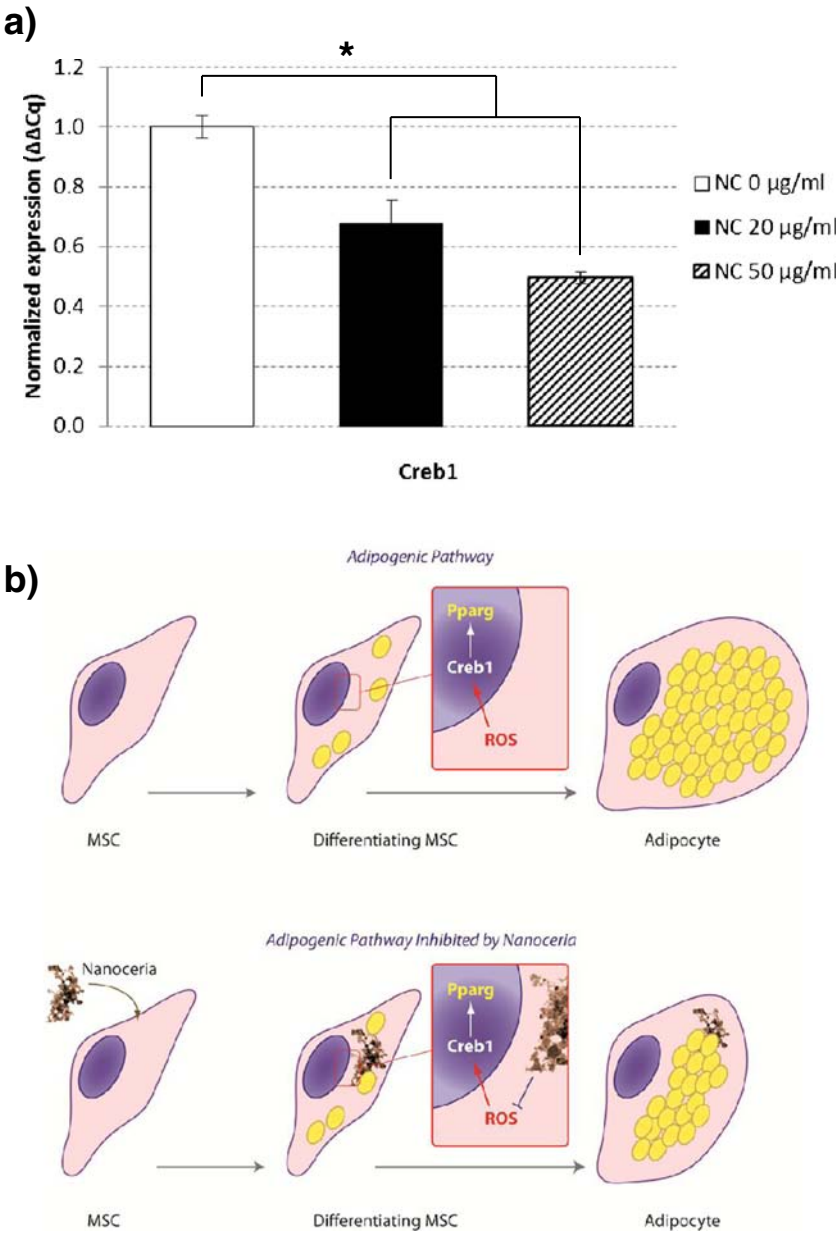

Fig. 8 Quantification of *Creb1* transcription through qRT–PCR after 14 days of differentiation of MSCs in the presence of NC; $*p < 0.05$ (**a**); schematization depicting the hypothesis of the inhibition of the adipogenic pathway caused by NC (**b**).

Cebpa activate several genes that are involved in the development of adipocytes, like lipoprotein lipase (coded by *Lpl*) and glycerol-3-phosphate dehydrogenase (coded by *Gpd1*) (38). In particular, the lipoprotein lipase has the function of hydrolyzing triglycerides in the early stage of adipogenesis (39), while glycerol-3-phosphate dehydrogenase is involved in the biosynthesis of lipids at the end of the adipocyte maturation (40).

Inhibitory effects of NC on adipogenesis were confirmed by the phenotype analysis of the cultures, both in terms of lipidic vesicles quantification and of G3PDH activity. This enzyme, in particular, catalyzes the conversion of glycerol-3-phosphate into dihydroxyacetone phosphate in the mitochondrial membrane (41). In cells treated with NC, the activity of G3PDH strongly decreased with respect to the control.

Taken together, these data suggest that the presence of NC inhibits the development of mature adipocytes (42). The mechanism of this effect is likely related to a ROS level reduction induced by the NC, that thus hinder a complete maturation of adipocytes. As widely recognized, NC in fact are able to reduce intracellular oxidative stress in several biological contexts (43–45). Plenty of researches delineate the involvement of the reactive oxygen species in the promotion of stem cell differentiation into mature adipocytes (46–48); as Supplementary Material we have reported ROS evaluation in proliferating MSCs and in differentiating MSCs, treated with NC and with *N*-acetyl-L-cysteine as anti-oxidant positive control, confirming high ROS production after adipogenesis induction, and its strong reduction when NC are

provided to the cells. The correlation between redox mechanism and adipogenesis was moreover proved by Kanda *et al.*, that identified cAMP response element-binding protein 1 (Creb1) as the transcription factor activated by ROS in MSCs (49). Creb1 is necessary to induce adipogenesis as it is involved in the transcriptional activation of *Pparg* (50). Hence, we hypothesized a possible pathway in which NC scavenge ROS, thus reducing the transcription of *Creb1* as confirmed by our qRT-PCR results (Fig. 8(a)), eventually hindering downstream activations that would lead to a complete adipocyte maturation (Fig. 8(b)).

CONCLUSIONS

In this study, we reported the behavior of MSCs differentiating toward adipocytes in the presence of NC, in terms of cytotoxic effects and adipogenic maturation. At the end of the experimental analysis, a clear decrement of adipogenesis was highlighted in cultures treated with NC at concentrations that do not affect their viability/proliferation. This effect, ascribable to the anti-oxidant properties of NC that scavenge the ROS necessary for a correct adipogenesis, represents an encouraging step toward NC-based therapy against obesity and other related metabolic syndromes.

REFERENCES

1. Celardo I, De Nicola M, Mandoli C, Pedersen JZ, Traversa E, Ghibelli L. Ce^{3+} Ions Determine redox-dependent anti-apoptotic effect of cerium oxide nanoparticles. ACS Nano. 2011;5:4537–49.
2. Karakoti AS, Munusamy P, Hostetler K, Kodali V, Kuchibhatla S, Orr G, *et al.* Preparation and characterization challenges to understanding environmental and biological impacts of ceria nanoparticles. Surf Interface Anal. 2012;44:882–9.
3. Korsvik C, Patil S, Seal S, Self WT. Superoxide dismutase mimetic properties exhibited by vacancy engineered ceria nanoparticles. Chem Commun (Camb). 2007;10:1056–8.
4. Heckert EG, Karakoti AS, Seal S, Self WT. The role of cerium redox state in the SOD mimetic activity of nanoceria. Biomaterials. 2008;29:2705–9.
5. Hirst SM, Karakoti AS, Tyler RD, Sriranganathan N, Seal S, Reilly CM. Anti-inflammatory properties of cerium oxide nanoparticles. Small. 2009;5:2848–56.
6. Pirmohamed T, Dowding JM, Singh S, Wasserman B, Heckert E, Karakoti AS, *et al.* Nanoceria exhibit redox state-dependent catalase mimetic activity. Chem Commun (Camb). 2010;46:2736–8.
7. Ciofani G, Genchi GG, Liakos I, Cappello V, Gemmi M, Athanassiou A, *et al.* Effects of cerium oxide nanoparticles on PC12 neuronal-like cells: Proliferation, differentiation, and dopamine secretion. Pharm Res. 2013;30:2133–45.
8. Ciofani G, Genchi GG, Mazzolai B, Mattoli V. Transcriptional profile of genes involved in oxidative stress and antioxidant defense in PC12 cells following treatment with cerium oxide nanoparticles. BBA Gen Subj. 1840;2013:495–506.
9. Niu J, Azfer A, Rogers LM, Wang X, Kolattukudy PE. Cardioprotective effects of cerium oxide nanoparticles in a transgenic murine model of cardiomyopathy. Cardiovasc Res. 2007;73:549–59.
10. Wason MS, Zhao J. Cerium oxide nanoparticles: potential applications for cancer and other diseases. Am J Transl Res. 2013;5:126–31.
11. Das M, Patil S, Bhargava N, Kang JF, Riedel LM, Seal S, *et al.* Autocatalytic ceria nanoparticles offer neuroprotection to adult rat spinal cord neurons. Biomaterials. 2007;28:1918–25.
12. Rodrigo R, Guichard C, Charles R. Clinical pharmacology and therapeutic use of antioxidant vitamins. Fundam Clin Pharmacol. 2007;21:111–27.
13. Firuzi O, Miri R, Tavakkoli M, Saso L. Antioxidant therapy: current status and future prospects. Curr Med Chem. 2011;18:3871–88.
14. Carillon J, Rouanet JM, Cristol JP, Brion R. Superoxide dismutase administration, a potential therapy against oxidative stress related diseases: several routes of supplementation and proposal of an original mechanism of action. Pharm Res. 2013;30:2718–28.
15. Estevez AY, Erlichman JS. Cerium oxide nanoparticles for the treatment of neurological oxidative stress diseases. In: oxidative stress: diagnostics, prevention, and therapy, ACS symposium series 2011;1083:255-288.
16. Celardo I, Traversa E, Ghibelli L. Cerium oxide nanoparticles: a promise for applications in therapy. J Exp Ther Oncol. 2011;9:47–51.
17. Valko M, Leibfritz D, Moncol J, Cronin MT, Mazur M, Telser J. Free radicals and antioxidants in normal physiological functions and human disease. Int J Biochem Cell Biol. 2007;39:44–84.
18. Valko M, Rhodes CJ, Moncol J, Izakovic M, Mazur M. Free radicals, metals and antioxidants in oxidative stress-induced cancer. Chem Biol Interact. 2006;160:1–40.
19. Brieger K, Schiavone S, Miller Jr FJ, Krause KH. Reactive oxygen species: from health to disease. Swiss Med Wkly. 2012;142:w13659.
20. Urakawa H, Katsuki A, Sumida Y, Gabazza EC, Murashima S, Morioka K, *et al.* Oxidative stress is associated with adiposity and insulin resistance in men. J Clin Endocrinol Metab. 2003;88:4673–6.
21. Evans JL, Goldfine ID, Maddux BA, Grodsky GM. Are oxidative stress-activated signaling pathways mediators of insulin resistance and beta-cell dysfunction? Diabetes. 2003;52:1–8.
22. Furukawa S, Fujita T, Shimabukuro M, Iwaki M, Yamada Y, Nakajima Y, *et al.* Increased oxidative stress in obesity and its impact on metabolic syndrome. J Clin Invest. 2004;114:1752–61.
23. Lee H, Lee YJ, Choi H, Ko EH, Kim JW. Reactive oxygen species facilitate adipocyte differentiation by accelerating mitotic clonal expansion. J Biol Chem. 2009;284:10601–9.
24. De Marchi E, Baldassari F, Bononi A, Wieckowski MR, Pinton P. Oxidative stress in cardiovascular diseases and obesity: role of p66Shc and protein kinase C. Oxid Med Cell Longev. 2013;2013:564961.
25. Savini I, Catani MV, Evangelista D, Gasperi V, Avigliano L. Obesity-associated oxidative stress: strategies finalized to improve redox state. Int J Mol Sci. 2013;14:10497–538.
26. Everard A, Cani PD. Diabetes, obesity and gut microbiota. Best Pract Res Clin Gastroenterol. 2013;27:73–83.
27. Ioannides-Demos LL, Piccenna L, McNeil JJ. Pharmacotherapies for obesity: past, current, and future therapies. J Obes. 2011;2011:179674.
28. Vetter ML, Faulconbridge LF, Webb VL, Wadden TA. Behavioral and pharmacologic therapies for obesity. Nat Rev Endocrinol. 2010;6:578–88.
29. Janderová L, McNeil M, Murrell AN, Mynatt RL, Smith SR. Human mesenchymal stem cells as an in vitro model for human adipogenesis. Obes Res. 2003;11:65–74.
30. Celardo I, Pedersen JZ, Traversa E, Ghibelli L. Pharmacological potential of cerium oxide nanoparticles. Nanoscale. 2011;3:1411–20.

31. Subash-Babu P, Alshatwi AA. Aloe-emodin inhibits adipocyte differentiation and maturation during in vitro human mesenchymal stem cell adipogenesis. J Biochem Mol Toxicol. 2012;26:291–300.
32. Chen S, Hou Y, Cheng G, Zhang C, Wang S, Zhang J. Cerium oxide nanoparticles protect endothelial cells from apoptosis induced by oxidative stress. Biol Trace Elem Res. 2013;154:156–66.
33. Dowding JM, Das S, Kumar A, Dosani T, McCormack R, Gupta A, *et al.* Cellular interaction and toxicity depend on physicochemical properties and surface modification of redox-active nanomaterials. ACS Nano. 2013;7:4855–68.
34. Niu J, Wang K, Kolattukudy PE. Cerium oxide nanoparticles inhibit oxidative stress and nuclear factor-κB activation in H9c2 cardiomyocytes exposed to cigarette smoke extract. J Pharmacol Exp Ther. 2011;338:53–61.
35. Singh S, Kumar A, Karakoti A, Seal S, Self WT. Unveiling the mechanism of uptake and sub-cellular distribution of cerium oxide nanoparticles. Mol Biosyst. 2010;6:1813–20.
36. Asati A, Santra S, Kaittanis C, Perez JM. Surface-charge-dependent cell localization and cytotoxicity of cerium oxide nanoparticles. ACS Nano. 2010;4:5321–31.
37. Lefterova MI, Lazar MA. New developments in adipogenesis. Trends Endocrinol Metab. 2009;20:107–14.
38. Farmer SR. Transcriptional control of adipocyte formation. Cell Metab. 2006;4:263–73.
39. Schilling T, Nöth U, Klein-Hitpass L, Jakob F, Schütze N. Plasticity in adipogenesis and osteogenesis of human mesenchymal stem cells. Mol Cell Endocrinol. 2007;271:1–17.
40. Urs S, Smith C, Campbell B, Saxton AM, Taylor J, Zhang B, *et al.* Gene expression profiling in human preadipocytes and adipocytes by microarray analysis. J Nutr. 2004;134:762–70.
41. Kim YH, Park TC, Lee G, Shin JC. Gene expression pattern of human chorion-derived mesenchymal stem cells during adipogenic differentiation. Yonsei Med J. 2012;53:1036–44.
42. Schiller ZA, Schiele NR, Sims JK, Lee K, Kuo CK. Adipogenesis of adipose-derived stem cells may be regulated *via* the cytoskeleton at physiological oxygen levels in vitro. Stem Cell Res Ther. 2013;4:79.
43. Pagliari F, Mandoli C, Forte G, Magnani E, Pagliari S, Nardone G, *et al.* Cerium oxide nanoparticles protect cardiac progenitor cells from oxidative stress. ACS Nano. 2012;6:3767–75.
44. Schubert D, Dargusch R, Raitano J, Chan SW. Cerium and yttrium oxide nanoparticles are neuroprotective. Biochem Biophys Res Commun. 2006;342:86–91.
45. Das S, Singh S, Dowding JM, Oommen S, Kumar A, Sayle TX, Saraf S, Patra CR, Vlahakis NE, Sayle DC, Self WT, Seal S. The induction of angiogenesis by cerium oxide nanoparticles through the modulation of oxygen in intracellular environments. Biomaterials 201;33:7746-55.
46. Liu GS, Chan EC, Higuchi M, Dusting GJ, Jiang F. Redox mechanisms in regulation of adipocyte differentiation: beyond a general stress response. Cells. 2012;1:976–93.
47. Tormos KV, Anso E, Hamanaka RB, Eisenbart J, Joseph J, Kalyanaraman B, *et al.* Mitochondrial complex III ROS regulate adipocyte differentiation. Cell Metab. 2011;14:537–44.
48. Kim DH, Puri N, Sodhi K, Falck JR, Abraham NG, Shapiro J, *et al.* Cyclooxygenase-2 dependent metabolism of 20-HETE increases adiposity and adipocyte enlargement in mesenchymal stem cell-derived adipocytes. J Lipid Res. 2013;54:786–93.
49. Kanda Y, Hinata T, Kang SW, Watanabe Y. Reactive oxygen species mediate adipocyte differentiation in mesenchymal stem cells. Life Sci. 2011;89:250–8.
50. Fox KE, Fankell DM, Erickson PF, Majka SM, Crossno Jr JT, Klemm DJ. Depletion of cAMP-response element-binding protein/ATF1 inhibits adipogenic conversion of 3T3-L1 cells ectopically expressing CCAAT/enhancer-binding protein (C/EBP) alpha, C/EBP beta, or PPAR gamma 2. J Biol Chem. 2006;281:40341–53.